ITC 3/54
Information Technology and Control
Vol. 54 / No. 3/ 2025
pp. 796-809
DOI 10.5755/j01.itc.54.3.38718

Complex Texture Segmentation of Digital Painting Image Based on Widow-HoffLMS Adaptive Algorithm

Received 2024/09/04 | Accepted after revision 2025/03/12

HOW TO CITE: Xue, Y. (2025). Complex Texture Segmentation of Digital Painting Image Based on Widow-HoffLMS Adaptive Algorithm. *Information Technology and Control*, 54(3), 796-809. https://doi.org/10.5755/j01.itc.54.3.38718

Complex Texture Segmentation of Digital Painting Image Based on Widow-HoffLMS Adaptive Algorithm

Yuanyuan Xue
School of Humanities and Law, Zhengzhou Technology and Business University, Zhengzhou 45000, China

Corresponding author: xue901213680829@163.com

When digital painting images are constructed to ensure a better visual effect of an image, it is necessary to carry out targeted processing on different areas of an image. So, image segmentation is a basis to ensure this processing effect. Therefore, this study proposes a method, called Widow-HoffLMS, for conducting complex texture segmentation for digital painting images. Firstly, the proposed algorithm is used to filter and process digital painting images, and the processing capability of the Hammerstein spline optimization algorithm is introduced to avoid damaging texture details of images and ensure detailed integrity of images. Then, filtered digital painting images are input into the adaptive network based on ghost convolution. A Ghost Module functions as an image block for convolutional neural networks that aims to generate more attributes by utilizing fewer parameters. After texture features in images are extracted through the ghost convolution layer of the network, the feature map is fused and extracted through the U-Net segmentation layer. Finally, the decoder is implemented to restore the spatial resolution of images and produce the result of complex texture segmentations of digital painting images. The test results show that the filtering effect of the proposed method is good, and the contrast of the filtered digital painting image is above 0.932. Moreover, the proposed method can complete the texture feature extraction of images with different sizes and different pixel scores, and the results of the inverse variance are all below 0.018. Furthermore, the complex texture segmentation of animated digital images can be completed according to the preset needs. The integrity state of the complex texture segmentation is also high.

KEYWORDS: Widow-HoffLMS adaptive algorithm, Digital painting image, Complex texture, Segmentation, Ghost convolution, Feature extraction.

1. Introduction

Digital painting images are works of art created using digital technology and software and have been widely used in illustration, animation, game design, movie special effects, advertising design, and art education [1]. These images do not rely on conventional painting media, such as paint, canvas, or paper, but are generated and edited entirely digitally. Digital painting images have many advantages that conventional painting does not have, such as editability, copying and sharing, layering, and compositing properties [2].

During the production and processing of digital painting images, texture, as one of the important visual features in an image, not only reflects the surface structure and material properties of the object but also plays a crucial role in understanding, analyzing, and recognizing an image. Texture segmentation is an important link, which can provide substantial basic data for subsequent image processing tasks (e.g. recognition, classification, compression) [3]. An image region obtained through texture segmentation can be used as input data for subsequent tasks, which can further improve the accuracy and efficiency of these tasks. At the same time, different regions in an image can be targeted processing through texture segmentation, such as enhancement, and suppression to improve the visual effect of an image [4].

However, due to the diversity and complexity of textures, conventional image segmentation methods often make it difficult to accurately segment regions with similar textures [5]. For this reason, to better achieve image segmentation, texture characterization technology based on light polarization characteristics is employed for texture characterization, and image pixel scores are expressed through different polarization characteristics to complete local texture segmentation [6]. However, the method requires the deployment of circular polarization filters and multi-angle rotation in an image acquisition process (such as one step every 10 degrees from 0 to 360 degrees), which requires the image acquisition equipment to have high accuracy and stability. In an environment of uneven illumination or strong reflection, changes in polarization characteristics may become complex and difficult to capture accurately, affecting the segmentation effect. To better achieve effective image segmentations based on the skeleton of over-segmented images, an adaptive Markov Random Field (MRF) method is used to process and extract the color and features of images, and then process them into hyper-pixels to achieve image segmentations better [7]. Although the adaptive MRF can deal with the local dependency between pixels, it may not be ideal for the long-distance dependency, namely, interactions between pixels that are far away in images, especially when dealing with images with complex textures, blurred edges, or low contrast. The segmentation results are excessively smooth or inaccurate in some areas. To better achieve image segmentations, a parallel algorithm for parallel apriori simple linear iterative clustering (SLIC) on Apache Spark is proposed [8]. This algorithm uses the operations in Apache Spark to achieve parallel processing of images, relies on image partitions to achieve parallel processing, obtains the shape and location characteristics of images, and partition images according to the feature results. However, a simple uniform partition may not fully consider the shape, size, and location of objects in an image, which leads to inaccurate segmentation results.

The article subsequently proposed an improved parallel apriori simple linear iterative clustering (PASLIC)-on-Spark algorithm to improve the accuracy by considering the shape and location of clusters in an image partition and controllable boundary repetition. The partition strategy itself still limits this improvement. To effectively perform image segmentations, a hybrid whale optimization algorithm with a novel local minimum avoidance method is proposed for multi-level threshold color image segmentation [9]. This method employs local minimum to segment an image to form multiple regions, to complete image segmentations, and utilizes the whale algorithm to optimize the optimal threshold. To enhance the segmentation effect, however, in multi-threshold color image segmentation, the algorithm needs to accurately detect the boundaries between different color or texture regions. However, due to the complexity of the color transition region of an image, the algorithm may find it difficult to accurately distinguish boundaries, resulting in rough or unsmooth segmentation edges.

Texture not only reflects the surface structure and material properties of the object but also plays a crucial role in understanding, analyzing, and recognizing an image. So, texture segmentation provides substantial basic data for subsequent image processing tasks. An image region obtained through texture segmentation can be implemented as input data for subsequent tasks and can further improve the accuracy and efficiency of these tasks. However, the diversity and complexity of textures lead conventional image segmentation methods to make it difficult to accurately segment regions with similar textures and require implementing different methodologies to complete local texture segmentation.

The Widow-Hoff LMS adaptive algorithm is widely used in signal processing, adaptive filtering, and other fields due to its simplicity, robustness, and easy implementation. The algorithm is primarily used for supervised learning where the system iteratively tunes the parameters to approximate a desired target function. It operates by adjusting the weights of the linear predictor so that the predicted output converges to the real output over time. The least mean squares (LMS) adaptive algorithm minimizes the mean square error (MSE) to constantly adjust the weight of the filter to achieve the optimal filtering effect. This feature gives the LMS algorithm potential application scope in the field of image processing, especially in scenes that need adaptive adjustment of parameters [10]. Therefore, according to the filtering effect of the LMS adaptive algorithm and the difficulties and requirements of complex texture segmentation of digital painting images, this research proposes a complex texture segmentation algorithm of digital painting images based on the Widow-HoffLMS adaptive algorithm. The contributions are: 1. The filtering effect of the proposed method is good, and the contrast of the filtered digital painting image is above 0.932, 2. The proposed method can complete the texture feature extraction of images with different sizes and different pixel scores, and the results of the inverse variance are all below 0.018, 3. The complex texture segmentation of animated digital images can be completed according to the preset needs, 4. The integrity state of the complex texture segmentation is also high. More up-to-date research can be found in [30-35].

2. A Complex Texture Segmentation of Digital Painting Images

2.1. Filtering Processing of Digital Painting Images Based on Widow-HoffLMS Adaptive Algorithm

2.1.1. A Functional Structure of Widow-HoffLMS Adaptive Algorithm

Digital painting images are often acquired by sensors on devices such as digital drawing boards, tablet PCs, or computers, which are affected by various factors during operation, such as sensor material properties, electronic components, and circuit structures, thus introducing noise. Common sensor noise includes thermal noise caused by resistance, channel thermal noise of field effect tube, photon noise, dark current noise, optical response non-uniformity noise, etc. [11]. In addition, improper human operation (e.g., wrong parameter settings, and inappropriate image processing steps) may also lead to image noise [12]. Therefore, an image should be filtered before running segmentation.

The Widow-HoffLMS adaptive algorithm realizes dynamic adaptation to image features by continuously adjusting the filter efficiency to minimize the output error as an optimization algorithm based on the gradient descent method. In image segmentation, image features such as color, texture, and shape may change due to different image contents [13]. The adaptability of the LMS algorithm enables it to cope with these changes and better realize image processing flexibly. To improve the accuracy and robustness of the segmentation process [14] this paper uses the Widow-HoffLMS adaptive algorithm to filter it before the complex texture segmentation of digital painting images is conducted. The functional structure of the Widow-HoffLMS adaptive algorithm is shown in Figure 1.

This algorithm is used for processing a digital painting image. The input $x(t)$ is plugged into the algorithm (original digital painting images). The output $y(t)$ is a processed digital painting image. The noise , the axial head weight $w(t)$ coefficients of the adaptive filter, the output error $e(t)$, and the desired result $q(t)$ are provided. During the operation of the Widow-HoffLMS adaptive algorithm, the system weight is adjusted

Figure 1
A Functional Structure of The Ridrow HougLMS Adaptive Algorithm.

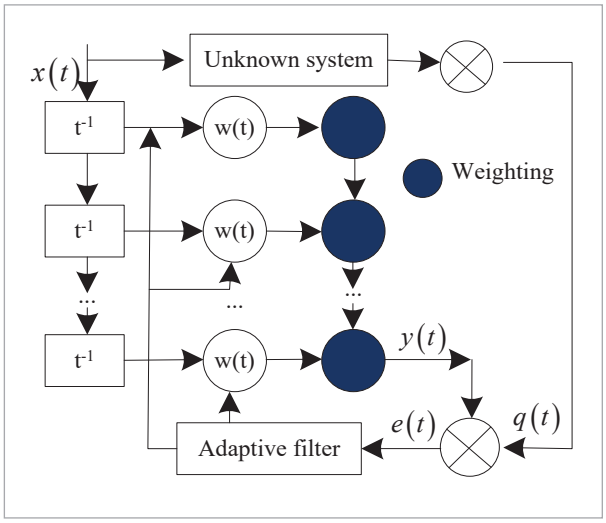

along the negative gradient direction, and the MSE is replaced by the squared error score, whose iterative computations are given as follows:

$$y(t) = w^t(t)x(t) \tag{1}$$

$$e(t) = q(t) - y(t) \tag{2}$$

$$w(t+1) = w(t) + 2\mu e(t)x(t), \tag{3}$$

where μ represents the iterative step factor to make the algorithm converge, the step factor μ takes scores satisfying $1 \le \mu \le \lambda_{\max}$ constraints, where represents the maximum eigenvalue $\lambda_{\max}$ of the autocorrelation matrix $x(t)$.

2.1.2. The Optimization of Widow-HoffLMS Adaptive Algorithm Based on Hammerstein Spline

Due to the high variety of colors and the structural complexity of digital painting images, it is necessary to ensure image detail integrity in processing [15]. Therefore, to improve the processing effect of the Widow-HoffLMS adaptive algorithm for digital painting images, the algorithm is optimized by using the Hammerstein spline to form a Hammerstein Spline Adaptive Filter-Least Mean Square (SAF-LMS) mainly composed of a memoryless nonlinear spline interpolation function based on adaptive look-up table and a linear adaptive filter.

In this study, we first interpolate the input $x(t)$, then obtain the nonlinear image processing result $s(t)$, and then the final output $y(t)$ is attained by processing $s(t)$ through a linear adaptive filter. Among them, the essence of nonlinear interpolation is to store the control points of the adaptive spline curve in the adaptive look-up table, and according to the score of the input image on the adaptive spline curve indexed to the appropriate interpolation point as the filter in t moment nonlinear output $s(t)$. The final output of the filter is obtained by calculating several nonlinear outputs and then filtering them linearly.

Because the first derivative of a cubic polynomial spline curve is continuous, has good smoothness, and considers the complexity of the algorithm, this paper uses a cubic polynomial curve as an interpolation spline curve. Both the B-spline curve and CR spline curve are commonly used as cubic polynomial curves, among which the CR spline curve can traverse all control points, which can make the algorithm more robust. Therefore, the CR spline curve is implemented as the nonlinear interpolation function in this filter. The span index of the control point needs to be computed before indexing the control point ξ and normalized horizontal coordinates ψ_t. In the case of uniform control point spacing and a third-order spline curve, the span index ξ and the normalized horizontal coordinates g_t are calculated as follows:

$$g_t = \frac{x(t)}{\Delta x} = \left\lfloor \frac{x(t)}{\Delta x} \right\rfloor \tag{4}$$

$$\xi = \left\lfloor \frac{x(t)}{\Delta x} \right\rfloor + \frac{M-1}{2}, \tag{5}$$

where $\lfloor\ \rfloor$, M, Δx represent downward rounding, the number of control points on the spline curve, the spacing between neighboring control points, and the control points of the spline curve. $M_n = [m_{x,i}, m_{y,i}]$ ($i \in [0, M]$ denotes M+1 control points of the spline curve, which is uniformly distributed in axis, and therefore arbitrarily satisfies $m_{x,0} < m_{x,1} < m_{x,2} < \cdots < m_{x,M}$ and therefore arbitrarily i satisfy $\Delta x_i = m_{x,i+1} - m_{x,i}$. After calculating the spanning index ξ and normalized horizontal coordinates ψ_t, the nonlinear output is given by:

$$s(t) = \varphi_i(t_n) = g_t^T C q_i(t), \tag{6}$$

where $g_t = [g_t^3, g_t^2, g_t^1, 1]$ and $d_i(t) = [d_{y,i}, d_{y,i+1}, d_{y,i+2}, d_{y,i+3}]^T$ vector represents the vertical coordinate of the control point indexed in the adaptive look-up table, $\phi(\cdot)$ represents a local spline function and is the CR spline basis matrix.

After obtaining the nonlinear output, the final output $y(t)$ can be obtained by the linear adaptive filter calculated as follows:

$$y(t) = w_n^T s(t), \tag{7}$$

where $w_t = [w(0), w(1), \cdots, w(M-1)]^T$ represents weighting factors for momentary linear adaptive filters at the time of t.

Errors $e(t)$ are calculated as follows:

$$e(t) = q(t) - y(t). \tag{8}$$

Based on the error signal $e(n)$, the approximate cost function is obtained as follows:

$$e(t)^2 = J[w(t), q_i(t)]. \tag{9}$$

To minimize the cost function, the cost function is sampled by the random gradient method, and the cost function is used to calculate the partial derivatives of the weight factor vector and the ordinate of the index control point respectively, then $w(t)$ in the spline adaptive filter-least mean square (SAF-LMS) algorithm is delineated by

$$w_{t+1} = w_t + \mu_2 e(t) s(t) \tag{10}$$

$$q_i(t+1) = q_i \mu_1 e(t) C^T U_{i,t} w_t, \tag{11}$$

where μ_1 and μ_2 represent the learning step of the adaptive spline curve, and the control points of the learning step of the linear adaptive filter weight factors, respectively; $U_{i,t}$ represent a matrix of digital painting images.

To summarize, digital drawing images $x(n)$ are input after nonlinear interpolation and linear adaptive filter processing to obtain the output digital drawing image $y(n)$, the update of the adaptive look-up table and linear adaptive filter weight factors is accomplished through Equation (11), and the next iteration is started, thus the digital painting image processing $x(n)$ is completed.

2.2. Texture Segmentation of Digital Painting Images Based on Ghosted Convolutional Adaptive Networks

2.2.1. The Overall Structure of the Texture Segmentation Model for Digital Painting Images

After the digital painting image processing is completed by following the steps above, the texture segmentation of the digital painting image is carried out. In this paper, the ghost convolution module is introduced based on the U-Net network to build a model that conducts texture segmentation of digital painting images, which is based on the adaptive ghost convolution. U-Net is a convolutional network architecture for fast and precise segmentation of images. Up to now, it has outperformed the prior best method. U-Net is developed for the task of semantic segmentation. When a neural network is fed images as inputs, this model uses the ghost convolution module to extract texture features of a digital painting image [16], and then texture segmentation is realized through the U-Net network to ensure that the texture features of an image are not damaged during segmentation [17]. Therefore, the constructed whole model consists of 2 parts. While one is the ghost convolution layer, the other is the U-Net segmentation layer. The overall structure of the model is shown in Figure 2.

Figure 2

The Structure of the Model Conducting: The Texture Segmentation of A Digital Painting Image Based on Ghost Shadow Convolutional Adaptive Network.

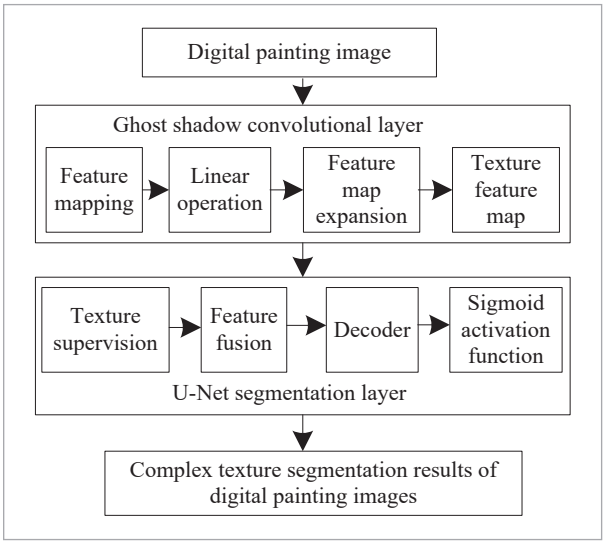

Ghosting Convolutional Layer

Convolutional neural networks (CNNs) expand the number of input feature maps through convolution layers, generating rich and even redundant information to ensure that the features of digital painting images can be fully extracted. However, redundant features also bring a lot of floating point operations (FLOPs) and model parameters, which lead to too long model training time and heavy memory consumption. After running ordinary convolution processing of digital painting images, there are a lot of similar structures like ghosts in Figure 2. This chapter uses ghost convolution to generate rich feature maps [18]. Ghost convolution uses cheap linear operations instead of some ordinary convolution operations, which can effectively reduce model parameters and better extract texture features of digital painting images.

U-Net Split Layer

U-Net is a U-shaped network structure that combines encoding and decoding processes. U-Net is a convolutional network architecture for fast and precise segmentation of images. Up to now, it has outperformed the prior best method. U-Net is developed for the task of semantic segmentation when a neural network is fed images as inputs. The encoding part is responsible for extracting image features and compressing them into vectors; In the decoding part, the compressed representation is transferred to a matrix to restore the spatial structure of an image. The transformed feature map is combined with the texture monitoring process, and the corrected texture features are obtained by back-propagation through the cross-entropy loss function. Finally, the correction results and the U-Net network segmentation feature map are normalized and combined to enhance texture features [19] to better realize the texture segmentation of digital painting images.

2.2.2. Texture Feature Extraction Based on Ghost Convolutional Layers

The ghost convolution layer consists of 2 parts: the first part of the ordinary convolution, the part of the strict control of the number of channels, the use of a limited number of filters on the input data of the channel and the space of the joint mapping output part of the feature map [20]. This feature map is called the fixed feature map. The second part of the ghost convolution: is the use of cheap linear operations to generate a fixed feature map that has similar characteristics to an image. This image is called the ghost feature map. The structure of a ghost convolution layer is shown in Figure 3.

Figure 3
The Convolutional Layer Structure of a Ghost Shadow.

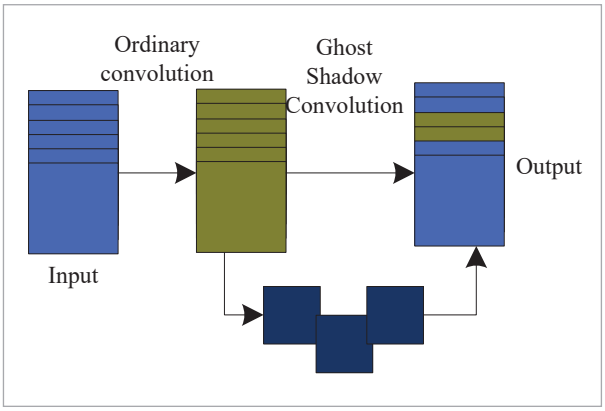

The detailed steps of the ghost convolutional layer for performing texture extraction of digitally painted images are described as follows:

Step 1: Ordinary convolution operation: Given the input data $y(n)$, whose height, width, and number of channels are denoted by H, W, and C, then the ordinary convolution for texture feature map extraction of digital painting image is calculated as:

$$y = L * y(t) + b \tag{12}$$

$$O_0 = R \times H \times W \times C \times K \times K, \tag{13}$$

where "*" represents the convolution operation, the set of output feature graphs is expressed in Y, the convolution filter set is expressed in L, the filter changes the number of data channels from C to R, the number of feature maps varies with the number of channels, $K \times K$ represents the size of the convolution kernel for ordinary convolution, O_0 represents the amount of ordinary convolutional floating-point arithmetic.

Step 2: Ghost convolution operation: a cheap linear operation $\Phi(\cdot)$ on a fixed digital painting image texture feature is a map O_Σ, the amount of calculation required to output S ghost feature maps is, which is calculated by:

$$Y_{ij} = \phi_{ij}(y_i') \quad \forall i, i = 1, \cdots, R; \quad j = 1, \cdots, r \tag{14}$$

$$O_{\Sigma} = R \times (r-1) \times H \times W \times \widehat{K} \times \widehat{K}, \tag{15}$$

where y'_i represents the i-th fixed feature graph in the output Y, y_{i1} represents the original image of the i-th fixed feature graph, $y_{ij(j\neq 1)}$ represents the j-th ghost feature graph of the fixed feature maps generated by cheap linear operation; R-th fixed feature graph finally output $N=R+R.\ (r–1)$ images, $\widehat{K} \times \widehat{K}$ represents the size of the convolution kernel of the ghost convolution and denotes the change of a fixed feature map into r–1 ghost feature map to complete the feature map expansion.

The ghost convolution layer can generate the texture feature map of the digital painting image just like the ordinary convolution layer, so it can easily replace the ordinary convolution layer to reduce the calculation cost of the model. In digital painting images with large sizes and high channels, the ghost convolution layer can significantly reduce the amount of computation. When compared with the ordinary convolution layer, which uses filter banks to output all the feature maps at one time, the ghost convolution layer uses a distributed structure to output the required feature maps one by one. First, a finite filter bank is used to jointly map the digital painting image to output a fixed texture feature map, and then a cheap linear operation is used to transform the fixed texture feature map into a ghost texture feature map. At the same time, the size of the ordinary convolution filter core is fixed, while the size of the ghost convolution filter core is diverse, which makes the feature mapping not in a single window sliding form, thus bringing more abundant texture feature maps of digital painting images $\tilde{Y} = \{\tilde{Y}_i, i \in [1,k]\}$, of which $\tilde{Y}_i \in C \times W \times H$, k denotes the number of multiple feature maps with different receptive fields. More up-to-date research can be found in [24-26].

2.2.3. U-Net Split Layer

The main function of the U-Net segmentation layer is to realize the texture segmentation of digital painting images. The module includes 2 steps in the whole segmentation process. While one is to fuse the texture feature map of the digital painting image extracted from the above summary, the other is to fuse the low-level features in the encoder with the decoder's high-level features through the decoder's jump connection to retain more detailed information. The spatial resolution of the image is restored, and the final result of complex texture segmentation of the digital painting image is generated.

To ensure the effect of feature fusion, the decoder of the U-Net segmentation layer realizes the fusion of texture feature maps of digital painting images through the Regional Adaptive Feature Integration Module (RAFS), to ensure the fusion effect between shallow features and deep features and ensure the comprehensive retention of complex texture features. At the same time, it increases the correlation between different feature maps and improves the accuracy of image segmentation prediction from feature integration.

After obtaining the input features, the decoder first fuses them through a 3×3 convolutional layer, and then combines the fused features with the predicted features through the designed channel reweighting block using element-wise addition operation. During the fusion process, to enable the model to adaptively select the feature information, a regional adaptive feature selection module is introduced, which is based on the feature dynamics adaptive selection mechanism, allowing each neuron to adaptively select feature information according to multiple scales or multiple receptive field sizes from different feature maps, and use the attention mechanism to fuse multiple feature maps with different receptive fields. As a given input feature map $\tilde{Y} = \{\tilde{Y}_i, i \in [1,k]\}$, its elements are summed up using Equation (16).

$$\tilde{Y}_i = \sum_{i=1}^{16} \tilde{Y}_i. \tag{16}$$

Global feature information is calculated by using global average pooling to generate channel statistics E, which are calculated by:

$$S = \eta\{P[z(E]\}, \tag{17}$$

where η represents the activation function; $z(E)$ represents the fully connected layer output; and P denotes the batch normalization process.

To preserve multiple texture feature maps of different receptive fields, cross-channel soft attention is selected to generate multiple weights adaptively through Softmax Attention. Equation (18) is used.

$$w_i = \frac{E_i}{\sum_i^k E_i}, \quad (18)$$

where w_i represents the attention weights for the I-th feature maps. Based on the attentional weights on the various receptive fields, matrix multiplication transformations were used to obtain new texture feature maps for digital painting images $\hat{Y}$, which are given by:

$$\hat{Y}_i = \{\hat{Y}_i \times w_i, i \in [1,k]\}. \quad (19)$$

Through the presented method above, the attention weight is learned to achieve automatic feature selection. Finally, the texture feature selection of the digital painting image by summing up each element is completed. At the end of the network is the Sigmoid activation function, which classifies the target texture and background to obtain the segmentation result image. Finally, the splicing and clipping results restore the spatial resolution of the image to obtain the final segmentation result of the complex texture of digital painting images. More research can be found in [27-32].

2.2.4. The Setting of Loss Function

In this subsection, the loss function is introduced to suppress the problem of uneven positive and negative samples, reduce the segmentation error caused by the small proportion of target texture pixels in the overall pixel of the image, and obtain excellent segmentation results. In this paper, the outputs of different module branches are fused according to the ratio effectively, so that the model can be reasonable, effective, and fully utilize the feature information in the training and prediction stages. The cross-entropy loss function is adopted as the loss function for the complex texture segmentation of digital painting images. Equation (20) is implemented.

$$X = -\sum_{i=1}^{N-1} y_i \log p_i, \quad (20)$$

where the partitioning y_i of real classes represents the predicted probability $p_i \in [0,1]$ of the model for the class of the segmentation label $y_i \ \ i = 1,\ldots,N$ and represents the total number of categories.

3. The Results of Testing and Analysis

To verify the application effect of the proposed method in the field of complex texture segmentation of digital painting images, this paper takes animations as digital painting images produced by a company specializing in animation productions to conduct relevant tests. There are obvious differences in the size of the images ranging from 50×50 pixels to 6000×4000 pixels, according to the application needs, the appropriate size images are selected to meet the needs of animation production. In this paper, 50 images of different sizes are randomly selected from the company's digital painting image database for testing. The extracted images contain different structural complexity and different colors to ensure the comprehensiveness and representativeness of the test results.

Parameter settings: the training batch size is set to 16, the number of training times is set to 100, the convolutional kernel size is 3×3, the initial learning rate is set to 0.001, the weight decay regular term is 0.0005, and the momentum parameter is 0.9.

The proposed method uses the Widow-HoffLMS adaptive algorithm to filter digital painting images before the complex texture segmentation of the digital painting image is run. To reliably judge the filtering effect of this algorithm, the contrast is used as the evaluation index, which is used to measure the clarity of the image texture and the depth of the texture grooves. So, this is used to judge whether the algorithm damages the texture structure of the image after filtering. The index score is between 0 and 1. The larger the score is, the deeper the texture grooves are, and the greater the contrast is, that is, the better the filtering effect is, the clearer the image is, and no damage occurs during filtering. Equation (21) is used to calculate the indicator.

$$K_O = \sum_i \sum_j (i-j)^2 p(i,j,d,\theta), \quad (21)$$

where i and j represent different pixels; d represents the statistical step size, and θ represents the statistical direction.

By the proposed method, 10 digital painting images of different sizes were filtered to test the processing of different degrees of image noise and obtain the results of the filtered images K_0. The results are shown in Table 1.

Table 1
Comparison of the test results of the filtered digital painting images.

Image size / pixel	Noise level /dB		
	3	6	9
50×50	0.943	0.952	0.963
200×200	0.951	0.971	0.948
400×400	0.967	0.968	0.972
800×800	0.946	0.977	0.968
1200×1200	0.938	0.941	0.989
1680×1680	0.966	0.957	0.977
2432×2432	0.973	0.956	0.966
2600×2600	0.932	0.967	0.954
3224×3224	0.985	0.981	0.949
6000×4000	0.976	0.983	0.952

Table 1 suggests that when there are different levels of noise in a digital painting image, the image results K_0 are all above 0.932, and the maximum is 0.989. Because the Widow-HoffLMS adaptive algorithm selects the Hammerstein spline to optimize the algorithm during image filtering, to better ensure its filtering effect and ensure the texture integrity after image processing.

The proposed method extracts the texture features of the image through the ghost convolutional layer when the complex texture segmentation of a digital painting image is carried out. To measure the extraction effect ofw the texture features, the inverse variance is used as a judgment criterion in the paper, which is capable of describing the degree of local change of the texture features, and takes a score between 0 and 1. If the texture of the image changes drastically in different regions, the inverse variance will be relatively small, indicating that the local change of the texture is larger and may contain more details or irregularities, therefore, the smaller the score of this index, the better the feature extraction effect is, and the more details can be obtained in the image. Equation (22) is used to calculate this index.

$$\mu = \sum_{i=1}^{N-1}\sum_{j=1}^{N-1}\frac{p(i,j\,|\,d,\theta)}{1+(i+j)^2}. \tag{22}$$

The texture features of digital painting images are extracted by the proposed method, and the result μ of the feature extraction with different numbers of pixels by the proposed method is obtained. The results are shown in Table 2.

Table 2
The Texture Feature Extraction of Digital Painting

Number of pixels/piece	Image size /pixel		
	50×50	1200×1200	6000×4000
100	0.017	0.011	0.011
200	0.016	0.014	0.012
300	0.015	0.012	0.009
400	0.018	0.015	0.01
500	0.016	0.013	0.013
600	0.012	0.011	0.012
700	0.014	0.013	0.014
800	0.015	0.014	0.011
900	0.013	0.016	0.012
1000	0.015	0.013	0.011

Table 2 suggests that the change in the number of pixels in the image indicates the higher complexity of the image structure under different image sizes, that is, the smaller the image size, the higher the number of pixels, which indicates the higher complexity of the image structure. After the application of the proposed method, the texture feature extraction of images with different sizes and pixel numbers can be completed, and the result of the inverse variance is less than 0.018. Even when the image size is the smallest 50×50 pixel and the number of pixels reaches 1000, the result of the inverse variance is only 0.015. Therefore, the proposed method has a better capability to extract complex texture features.

To verify the segmentation effect of the proposed method for the complex texture of digital painting images, 2 digital animation images (scene digital image and animal digital image, respectively) are randomly extracted from the selected test images for the texture segmentation test, and the complexity of the 2 images and the color structure are different, to analyze the segmentation effect of the proposed method in a more comprehensive way, and the segmentation results are shown in Figures 4-5, respectively. When

segmentation is performed, the segmentation target of Figure 4 is to obtain the complex texture segmentation results of the trees in the image and to obtain the texture segmentation results of the foreground in Figure 5.

After analyzing the test results of Figures 4-5, it is concluded that the target texture segmentation results of the images can be obtained according to the segmentation requirements, for example, the segmentation target in Figure 4 obtains the complex texture of the trees in the image, after the segmentation of 2 digitally drawn images with different complexity and color structure is run. The proposed method comprehensively obtains the texture segmentation results of the 2 trees in the scene image. The texture segmentation results, even if the distribution and structural complexity of the texture are high, can still reliably realize the segmentation. According to the foreground texture segmentation that completes the complex texture segmentation of the foreground animals and trees in the animated digital image, the complex texture segmentation of the two images is achieved with high completeness.

To further verify the segmentation effect of the proposed methods on the complex texture of digitally rendered images, the methods presented in [7-9] are

Figure 4

The texture segmentation results in scene digital images. (a) Image before segmentation and (b) Complex texture segmentation results.

(a) Image before segmentation

(b) Complex texture segmentation results

Figure 5

The texture segmentation results of animal digital images (a) Image before segmentation and (b) Texture result after segmentation.

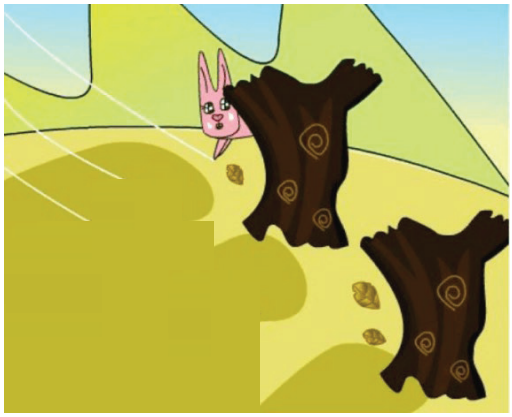

(a) Image before segmentation

(b) Texture result after segmentation

all used for comparison purposes. Complex texture segmentation is performed on digitally rendered images of different sizes through 4 methods, and the Dice coefficient is used as the evaluation index of the segmentation effect, The segmentation effect of the 4 methods is analyzed. The score is between 0 and 1. The larger the score is, the better the segmentation effect will be. Equation (23) is used to calculate this indicator.

$$C_D = \frac{2\left|X \cap Y\right|}{\left|X\right| + \left|Y\right|}, \tag{23}$$

where $2\left|X \cap Y\right|$ represents the same number of elements for samples X and Y, $|X|$ and $|Y|$ represents the total number of elements for samples X and Y; coefficient 2 represents the reason for repeating the common elements in samples. The segmentation effect analysis results of the methods in [7-9] are presented. The results are shown in Table 3.

Table 3 suggests that it is concluded that the complex texture segmentation of digital rendering images is carried out by 4 methods. When the same size of digital rendering image is segmented and the image size is small, the segmentation results of the methods in [7-9] are relatively good, and the Dice coefficient results are all above 0.847. With the increase in image size, the Dice coefficient results gradually decline. When the proposed method is used for complex texture segmentation of digital rendering images, the Dice coefficient results are all above 0.902, which can better complete complex texture segmentation. Even when the image size is large, the segmentation effect is still good.

4. Conclusion

Image segmentation is a basis to ensure the processing effect when digital painting images are constructed to ensure the visual effect of an image. Thus, it is necessary to carry out targeted processing on different areas of an image. Therefore, more complex segmentation methods are required to have better outcomes.

This paper proposes a method for conducting texture segmentation of digital painting images based on the Widow-HoffLMS adaptive algorithm when complex texture segmentation of digital painting images is needed.

After analyzing the application effect of the proposed method through testing, it is determined that it meets the needs of complex texture segmentation of digital painting images, can better complete the texture segmentation of digital painting images with different levels of complexity and noise, and can provide a reliable basis for targeted processing of different regions in the image.

The Dice coefficient results are greater than 0.847 when image size increases. Moreover, the proposed method helps segment complex texture segmenta-

Table 3
The analysis of segmentation effects of four methods.

Image size /pixel	Method in Reference [7]	Method in Reference [8]	Method in Reference [9]	Proposed Method
50×50	0.924	0.915	0.912	0.955
200×200	0.911	0.909	0.908	0.948
400×400	0.907	0.906	0.903	0.942
800×800	0.903	0.902	0.899	0.938
1200×1200	0.895	0.894	0.892	0.929
1680×1680	0.877	0.883	0.886	0.923
2432×2432	0.862	0.872	0.871	0.918
2600×2600	0.859	0.863	0.864	0.913
3224×3224	0.851	0.857	0.858	0.907
6000×4000	0.847	0.849	0.851	0.902

tions of digital rendering images with the Dice coefficient greater than.

It implies that better complete complex texture segmentation is achieved.

The limitation of the research is that the proposed method uses a linearity assumption. However, several implementations require non-linearity. Thus, several non-linear assumptions could be used to improve the results.

Future work will focus on other images used in different fields such as bio-medical images and the complexity of the algorithm will be reduced to be implemented in the practical applications.

Declaration of Conflicting Interests

The author declared no potential conflicts of interest concerning the research, authorship, and/or publication of this article.

References

1. Abdel-Basset, M., Mohamed, R., Abdelaziz, N. M., Abouhawwash, M. HWOA: A Hybrid Whale Optimization Algorithm With a Novel Local Minima Avoidance Method for Multi-Level Thresholding Color Image Segmentation. Expert Systems with Application, 2022, 190, 116145.1-116145.20. https://doi.org/10.1007/s11227-021-04027-5
2. Acarbay, E. Z., Zkurt, N. Performance Analysis of the Speech Enhancement Application with Wavelet Transform Domain Adaptive Filters. International Journal of Speech Technology, 2023, 26(1), 245-258. https://doi.org/10.1007/s10772-023-10022-3
3. Agbesi, V. K., Chen, W., Ukwuoma, C. C. ., Kuadey, N. A., Agbesi, C. C. M., Ejiyi, C. J. ., Gyarteng, E. S. A. ., Muoka, G. W. ., Kuadey, A. M. Multichannel 2D-CNN Attention-Based BiLSTM Method for Low-Resource Ewe Sentiment Analysis. Journal of Data Science and Intelligence. Systems, 2023, 3(1), 67-77. https://doi.org/10.47852/bonviewJDSIS32021512
4. Chandra, K. V., Bagadi, K. P., Sagar, K. V., Sri, R. M., Rani, K. S. Deep Learning-Powered Corneal Endothelium Image Segmentation with Attention U-Net.International Journal of Performability Engineering, 2023, 19(11), 736-743. https://doi.org/10.23940/ijpe.23.11.p4.736743
5. Chen, H., Ru, J., Long, H., He, J., Chen, T., Deng, W. Semi-Supervised Adaptive Pseudo-Label Feature Learning for Hyperspectral Image Classification in Internet of Things. In IEEE Internet of Things Journal, 2024, 11(19), 30754-30768. https://doi.org/10.1109/JIOT.2024.3412925
6. Deng, W., Wang, J., Guo, A., Zhao, H. Quantum Differential Evolutionary Algorithm with Quantum-Adaptive Mutation Strategy and Population State Evaluation Framework for High-Dimensional Problems. Information Sciences, 2024, 676, 120787. https://doi.org/10.1016/j.ins.2024.120787
7. Ghosh, S., Hassan, S. K. K., Khan, A. H., Manna, A., Sarkar, R. Application of Texture-Based Features for Text Non-Text Classification in Printed Document Images with Novel Feature Selection Algorithm. Soft Computing: A Fusion of Foundations, Methodologies, and Applications, 2022, 26(2), 891-909. https://doi.org/10.1007/s00500-021-06260-9
8. Gokul, P., Verma, U. Texture Based Prototypical Network for Few-Shot Semantic Segmentation of Forest Cover: Generalizing for Different Geographical Regions. Neurocomputing, 2022, 538(14), 126201.1-126201.8. https://doi.org/10.1016/j.neucom.2023.03.062
9. Hazarika, R. A., Maji, A. K., Syiem, R., Sur, S. N., Kandar, D. Hippocampus Segmentation Using U-Net Convolutional Network from Brain Magnetic Resonance Imaging (MRI). Journal of Digital Imaging: The Official Journal of the Society for Computer Applications in Radiology, 2022, 35(4), 893-909. https://doi.org/10.1007/s10278-022-00613-y
10. Huang, C., Wu, D., Zhou, X., Song, Y., Chen, H., Deng, W. Competitive Swarm Optimizer with Dynamic Multi-Competitions and Convergence Accelerator For Large-Scale Optimization Problems. Applied Soft Computing, 2024, 167(A), 112252. https://doi.org/10.1016/j.asoc.2024.112252
11. Kamalpreet, K., Renu D. Deep learning based hybrid ghost-net for metaspread chromosome image segmentation, Biomedical Signal Processing and Control, Volume 95, Part B, 2024, 106298, https://doi.org/10.1016/j.bspc.2024.106298
12. Kumari, A., Sahoo, S. K. An Effective and Robust Single-Image Dehazing Method Based on Gamma Correction and Adaptive Gaussian Notch Filtering. Journal of Supercomputing, 2024, 80(7), 9253-9276. https://doi.org/10.1007/s11227-023-05805-z

13. Kundu, S., Karale, V., Ghorai, G., Sarkar, G., Ghosh, S., Dhara, A. K. Nested U-Net for Segmentation of Red Lesions in Retinal Fundus Images and Sub-image Classification for Removal of False Positives. Journal of Digital Imaging: The Official Journal of the Society for Computer Applications in Radiology, 2022, 35(5), 1111-1119. https://doi.org/10.1007/s10278-022-00629-4

14. Longsong, Z., Liming, L., Xiaoqi S. GA-Net: Ghost Convolution Adaptive Fusion Skin Lesion Segmentation Network. Computers in Biology and Medicine, 2023, 164, 107273, https://doi.org/10.1016/j.compbiomed.2023.107273

15. Loverdos, D., Sarhosis, V. Automatic Image-Based Brick Segmentation and Crack Detection of Masonry Walls Using Machine Learning. Automation in Construction, 2022, 140, 104389.1-104389.15. https://doi.org/10.1016/j.autcon.2022.104389

16. Michieli, U., Zanuttigh, P. Edge-Aware Graph Matching Network for Part-Based Semantic Segmentation. International Journal of Computer Vision, 2022, 130(11), 2797-2821. https://doi.org/10.1007/s11263-022-01671-z

17. Mohammed, A. S., Mihoub, Z. A Review of Image Segmentation Strategies from Classical Methods to Deep Learning. 2024 Conference of Young Researchers in Electrical and Electronic Engineering (ElCon), Saint Petersburg, Russian Federation, 2024, 712-718. https://doi.org/10.1109/ElCon61730.2024.10468368

18. Nouri, M., Baleghi, Y. An Active Contour Model Reinforced by Convolutional Neural Network and Texture Description. Neurocomputing, 2023, 528, 125-135. https://doi.org/10.1016/j.neucom.2023.01.047

19. Okyere, F. G., Cudjoe, D., Sadeghi-Tehran, P., Virlet, N., Riche, A. B., Castle, M., Greche, L., Mohareb, F., Simms, D., Mhada, M. Machine Learning Methods for Automatic Segmentation of Images of Field- and Glasshouse-Based Plants for High-Throughput Phenotyping. Plants, 2023, 12(10), 2035. https://doi.org/10.3390/plants12102035

20. Oprisescu, S., Coliban, R. M., Ivanovici, M. Polarization-Based Optical Characterization for Color Texture Analysis and Segmentation. Pattern recognition letters, 2022, 163, 74-81. https://doi.org/10.1016/j.patrec.2022.09.019

21. Park, G., Heo, Y. S., Lee, K., Kwon, H. Y. A Parallel and Accurate Method for Large-Scale Image Segmentation on a Cloud Environment. Journal of Supercomputing, 2022, 78(3), 4330-4357. https://doi.org/10.1007/s11227-021-04027-5

22. Peng, B., Gao, D., Wang, M., Zhang, Y. 3D-STCNN: Spatiotemporal Convolutional Neural Network Based on EEG 3D Features for Detecting Driving Fatigue. Journal of Data Science and Intelligent Systems, 2023, 2(1), 1-13. https://doi.org/10.47852/bonviewJDSIS3202983

23. Priya, G. S., Padmapriya, N.PT-CNN: A Non-linear Lightweight Texture Image Classifier. Neural Processing Letters, 2023, 55(6), 8483-8507. https://doi.org/10.1007/s11063-023-11322-0

24. Punn, N. S., Agarwal, S. BT-Unet: A Self-Supervised Learning Framework for Biomedical Image Segmentation Using Barlow Twins with U-Net Models. Machine Learning, 2022, 111(12), 4585-4600. https://doi.org/10.1007/s10994-022-06219-3

25. Ran, X., Suyaroj, N., Tepsan, N., Ma, J., Zhou, X., Deng, W. A Hybrid Genetic-Fuzzy ant Colony Optimization Algorithm for Automatic K-means Clustering in an Urban Global Positioning System. Engineering Applications of Artificial Intelligence, 2024, 137(B), 109237. https://doi.org/10.1016/j.engappai.2024.109237

26. Reddy, E. S., Suneetha, A. Improved Generalised Fuzzy Peer Group with Modified Trilateral Filter to Remove Mixed Impulse and Adaptive White Gaussian Noise From Colour Images. International Journal of Nanotechnology, 2023, 20(1/4), 129-150. https://doi.org/10.1504/IJNT.2023.10056473

27. Sasmal, P., Bhuyan, M. K., Dutta, S., Iwahori, Y. An Unsupervised Approach of Colonic Polyp Segmentation Using Adaptive Markov Random Fields. Pattern recognition letters, 2022, 154, 7-15. https://doi.org/10.1016/j.patrec.2021.12.014

28. Simani, S., Lam, Y. P., Farsoni, S., Castaldi, P. Dynamic Neural Network Architecture Design for Predicting Remaining Useful Life of Dynamic Processes. Journal of Data Science and Intelligent Systems, 2023, 2(3), 141-152. https://doi.org/10.47852/bonviewJDSIS3202967

29. Subramanian, M., Lingamuthu, V., Venkatesan, C., Perumal, S.Content-Based Image Retrieval Using Colour, Gray, Advanced Texture, Shape Features, and Random Forest Classifier with Optimized Particle Swarm Optimization. International Journal of Biomedical Imaging, 2022, 1, 3211793-3211806. https://doi.org/10.1155/2022/3211793

30. Song, L., Cao, Y., Zhou, Y., You, D. A Denoising Algorithm Combined with EMD and LMS for Precise Transmission Signal. Shock and Vibration, 2023, 8853345. https://doi.org/10.1155/2023/8853345

31. Yao, L., Yankang, C., Zhouzhou, Z., Yingwei S., Mengmeng Z., Bin Y., Chengliang, T., Yan Z., GMetaNet: Multi-scale Ghost Convolutional Neural Network with Auxiliary Metaformer Decoding Path for Brain Tumor Segmentation. Biomedical Signal Processing and Control, 2023, 83, 104694. https://doi.org/10.1016/j.bspc.2023.104694

32. Zerouali, M., Djendi, M. A New Efficient Multi-Channel Fast NLMS (MC-FNLMS) Adaptive Algorithm for Audio Teleconferencing Systems. Physical Communication, 2024, 62, 102233.1-102233.12. https://doi.org/10.1016/j.phycom.2023.102233

33. Zhang, L.J., Qian, L. Y. Improved TCKF Algorithm Based on Noise Adaption and Square Root Filtering. Computer Simulation, 2022, 39(01), 322-326.

34. Zhao, H., Wang, L., Zhao, Z., and Deng, W. A New Fault Diagnosis Approach Using Parameterized Time-Reassigned Multisynchrosqueezing Transform for Rolling Bearings. In IEEE Transactions on Reliability. https://doi.org/10.1109/TR.2024.3371520

35. Zhu, Z., Li, X., Chen, H., Zhou, X., Deng, W. An Effective and Robust Genetic Algorithm with Hybrid Multi-Strategy and Mechanism for Airport Gate Allocation. Information Sciences, 2024, 654, 119892, https://doi.org/10.1016/j.ins.2023.119892